Abstract

We have obtained fully resolved spectra of the ν_1 (*Q*-branch) band of CF_4 at a pressure of 4 Torr using a variation of stimulated Raman spectroscopy. With an experimental resolution of ≤ 0.004 cm^{-1}, no detectable tensor splitting of the rotational levels exists up to $J = 55$. The spectrum is readily fit with a band origin $\alpha = 909.0720$ cm^{-1} and a single rotational term $\beta - \beta_0 = -3.417 \times 10^{-4}$ cm^{-1}. We have also observed an underlying hot band, which we tentatively assign as the $\nu_1 + \nu_2 \leftarrow \nu_2$ transition, with $\alpha' = 909.1997$ cm^{-1} and $(\beta - \beta_0)' = -3.405 \times 10^{-4}$ cm^{-1}.

JOURNAL OF MOLECULAR SPECTROSCOPY 86, 250–257 (1981)

Inverse Raman Spectrum of the ν_1-Fundamental of CF_4*

PETER ESHERICK AND ADELBERT OWYOUNG

Sandia National Laboratories, Albuquerque, New Mexico 87185

AND

CHRIS W. PATTERSON

University of California, Los Alamos Scientific Laboratories, Los Alamos, New Mexico 87545

We have obtained fully resolved spectra of the ν_1 (Q-branch) band of CF_4 at a pressure of 4 Torr using a variation of stimulated Raman spectroscopy. With an experimental resolution of ≤ 0.004 cm^{-1}, no detectable tensor splitting of the rotational levels exists up to $J = 55$. The spectrum is readily fit with a band origin $\alpha = 909.0720$ cm^{-1} and a single rotational term $\beta - \beta_0 = -3.417 \times 10^{-4}$ cm^{-1}. We have also observed an underlying hot band, which we tentatively assign as the $\nu_1 + \nu_2 \leftarrow \nu_2$ transition, with $\alpha' = 909.1997$ cm^{-1} and $(\beta - \beta_0)' = -3.405 \times 10^{-4}$ cm^{-1}.

INTRODUCTION

The recent development of stimulated and inverse Raman processes as techniques for obtaining ultra-high-resolution Raman spectra has resulted in the observation of a number of detailed Q-branch spectra of lighter spherical-top molecules (most notably methane and its isotopic derivatives) (*1–3*).

In this paper we describe a modification of the apparatus that allows us to probe Stokes shifts below 2000 cm^{-1}. This has led to the first observation of a fully resolved Q-branch Raman spectrum for a heavy molecule. We illustrate the modified technique by presenting here the inverse Raman spectrum (IRS) of CF_4 in the vicinity of the ν_1 Q-branch. This molecule was chosen as a continuation of our study of the spectroscopy of spherical tops. Although some rotational substructure has been previously observed at high J for other heavy spherical-top molecules, this is the first time in which the J rotational structure for essentially an entire Q-branch has been fully resolved for such a molecule. We shall include in this paper results, for the ν_1 band, and for underlying transitions which we have identified as the Q-branch of the $\nu_1 + \nu_2 \leftarrow \nu_2$ hot band.

EXPERIMENTAL APPARATUS

The apparatus used for these experiments closely parallels the quasi-cw inverse Raman apparatus described in Ref. (*3*). We overlap a pulsed pump laser and a cw probe laser in a focus in the gas sample and measure the transient signal induced

* This work was supported by the United States Department of Energy.

on the probe by the pulsed pump. Because the probe laser is on the shorter wavelength (anti-Stokes) side of the pump laser, the observed signal is an induced Raman absorption of the probe, i.e., an "inverse Raman" signal.

The pulsed pump laser source is a single-mode, electronically scannable cw dye oscillator (Coherent Model 599-021) which has been pulse amplified to 2 MW by three dye amplifiers pumped with a frequency-doubled Nd:YAG laser source. This system operates at a 10 pps repetition rate and emits pulses of <100 MHz spectral width (FWHM) and 6-nsec duration. In order to extend the range of this IRS technique to lower Raman shifts, the cw argon ion laser probe previously used was replaced by a single-mode, cw dye ring laser (Spectra Physics Model 380A). Pumped with 2.5 W from a single-mode argon ion laser, the Rh6G ring laser was able to provide up to 300 mW output with a linewidth and frequency stability of ± 20 MHz. Amplitude modulation on the ring laser output was found to be excessive when the argon ion pump laser was operated multimode. However, under single-mode pumping conditions, the noise level was reduced to about twice the shot noise limit. By using dye lasers for both the pump and probe, one can, in principle, tune their frequency differences essentially to zero cm^{-1}. In fact, the minimum practical Raman shift observable will be limited by the means used to separate the weak cw-probe signal from high intensity pulsed pump light at the detector. The Pellin–Broca prism, grating, and pinhole-pair system used here and in Ref. (*3*) was found to be perfectly adequate for a 900 cm^{-1} Raman shift. However, a double grating system in addition to a strongly crossed beam configuration may be required for significantly lower Stokes shifts. Nevertheless, discrimination is still expected to be orders of magnitude higher than that which is obtained in spontaneous Raman studies (*4*).

In addition to the different probe laser, the apparatus for these experiments also differed from Ref. (*3*) in the manner in which the data was recorded and analyzed. We have updated the apparatus by digitizing the data in real time and storing it in a microprocessor-based data acquisition system. With each laser shot, this system samples the output of a boxcar integrator, which measures the ratio of the transient absorption on the probe beam to the incident pump intensity, and averages an optional number of shots before storing the result. A second input channel is used to monitor the transmission of unamplified pump light through a 150-MHz confocal etalon. This channel provides the data set with a sequence of evenly spaced frequency markers as the pump source is scanned. At the end of a scan the data are permanently stored on a floppy disk for later retrieval and analysis. The latter is performed by transmitting the data to a CDC 6600 time-sharing system where it is wavenumber scaled and plotted, and peak positions are identified using a number of interactive programs (*5*) written in APL.

Absolute wavenumber calibration of the spectra was accomplished by using a cw wavemeter (*6*), with a microprocessor interface, which provided a continuous readout of the wavelengths of both pump and probe sources and their relative Raman shift. The addition of a phase-locked-loop frequency multiplier to the fringe counting electronics (*6*) of this device increased its resolution to about 5 parts in 10^8. The standard deviation for a number of measurements of the Stokes shift is typically 0.001 cm^{-1}.

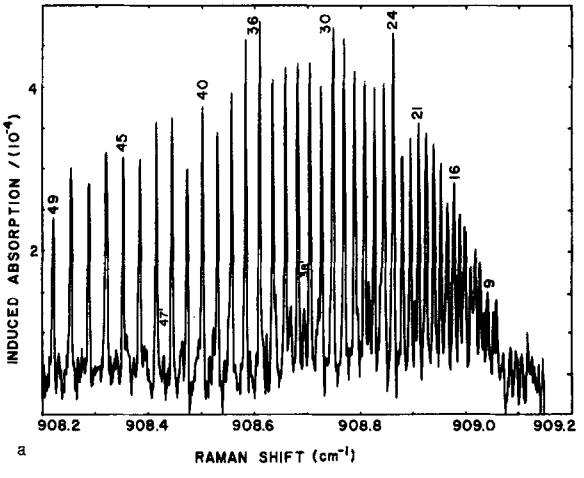

FIG. 1a. Observed Q-branch spectrum of ν_1 of CF_4 at 4 Torr, with a 1.5-MW pump laser, 300-mW probe laser. Time constant was 2 sec with a total scan time of 45 min.

RESULTS

The inverse-Raman Q-branch spectrum of the ν_1 band of CF_4 is shown in Fig. 1a. The spectrum was obtained at room temperature with 4 Torr of CF_4 in the sample cell. Resolution at this pressure was primarily limited by the pulsed-pump-source linewidth of 80 MHz. The spectrum is most remarkable in its simplicity. It is readily fit with only two parameters and shows no evidence for higher order terms even for $J > 50$.

An expanded spectrum of the band origin region is shown in Fig. 2a. From the figure it becomes apparent that what appears at first as noise in the compressed scan (Fig. 1a) is in fact very structured and periodic. Returning to Fig. 1a, the

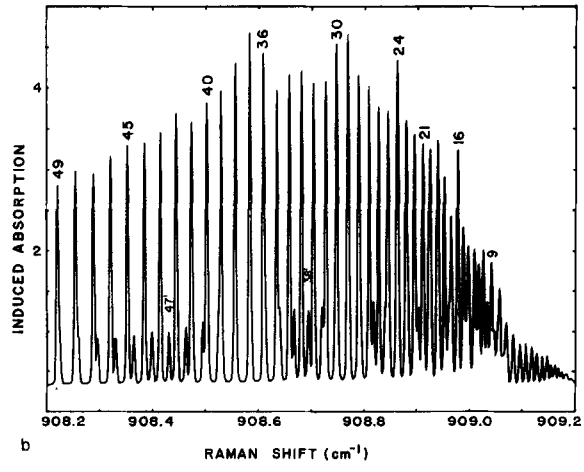

FIG. 1b. Simulated spectrum using calculated line positions and a 4.1×10^{-3} cm^{-1} FWHM Voight profile.

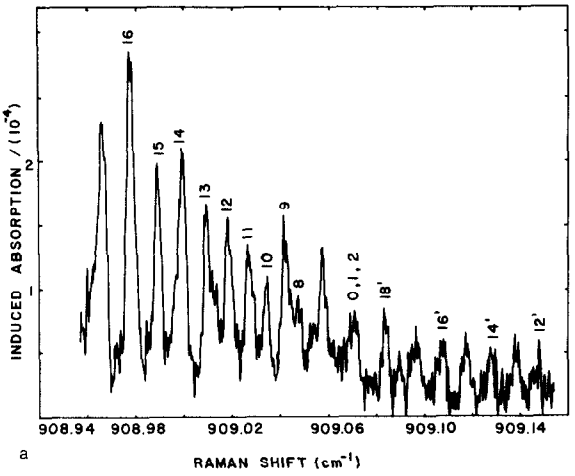

FIG. 2a. Observed spectrum near the ν_1 band origin, showing the weaker $\nu_2 + \nu_1 \leftarrow \nu_2$ progression identified by primed J values. Operating parameters as in Fig. 1a with the exception of time constant which was 10 sec.

periodic appearance of weak peaks is also apparent elsewhere in the spectrum, particularly between $J = 30$ and 36 and between $J = 40$ and 45. We have identified these weaker transitions as members of the Q-branch of the $\nu_1 + \nu_2 \leftarrow \nu_2$ hot band. We shall show that by including this band in a simulation of the spectrum (Figs. 1b and 2b) we are able to reproduce remarkably well the intensities of transitions throughout the spectrum.

The first step in simulating the spectrum is to parameterize the measured line positions of each peak. For a spherical top, these frequencies should be given to

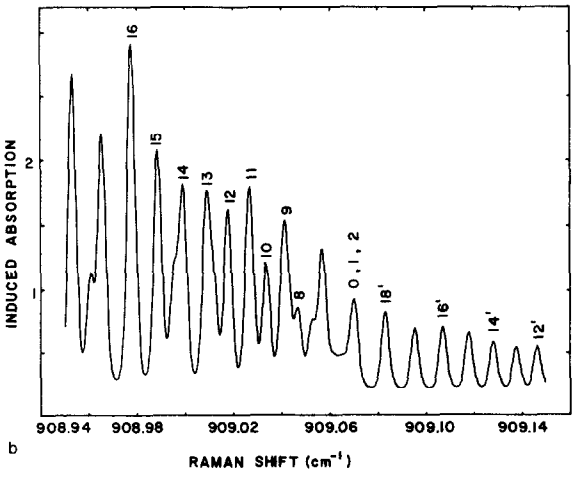

FIG. 2b. Simulated spectrum with 3.5×10^{-3} cm^{-1} FWHM Voight profile. Note the variation of intensity from a smooth function of J due to both the presence of overlapping bands and variation of the spin statistical weights for each line.

second order in the Hamiltonian by the expression (7)

$$\nu = \alpha + (\beta - \beta^0)J(J+1) + (\gamma - \gamma^0)J^2(J+1)^2 + (\epsilon - \epsilon^0)(-1)^J \times [(2J-3)(2J-2)\cdots(2J+5)]^{1/2}F^{4JJ}_{A_1pp}, \quad (1)$$

where the final term describes the tensor splitting of a given J level.

Starting with the ν_1 band transitions, we took 42 fully resolved rotational lines (J = 10 to 51) measured from nine separate scans similar to that shown in Fig. 1a. The assignment of J for these transitions was basically by trial and error, verified in the end by comparison of intensities. Performing a linear least-squares fit on this data, we found that we could fit the 42 measured frequencies with an overall rms deviation of only $\sigma = 3.2 \times 10^{-4}$ cm^{-1} by using just the first two terms of Eq. (1). Varying our assignment of J by either +1 or −1 caused a fivefold increase in this standard deviation. The best fit parameters obtained in this manner for our assigned J were

$$\alpha = 909.0720 \pm 0.0001 \text{ cm}^{-1},$$

$$\beta - \beta^0 = (-3.417 \pm 0.0006) \times 10^{-4} \text{ cm}^{-1},$$

where the uncertainties given are based solely on the "goodness of fit." Absolute accuracy of the band origin parameter, α, is of course limited by the absolute accuracy of our wavemeter, which is of the order 0.001 cm^{-1}. Table I lists the observed and calculated line positions as a function of J based on these parameters, as well as relative line intensities.

With the spectral resolution that we have been able to achieve to date, we have not been able to determine the last two constants in Eq. (1). For example, attempts to include a $J^2(J+1)^2$ term do not improve the fit and result in a value for $(\gamma - \gamma^0)$ that is smaller than the calculated uncertainty for that parameter. By making careful measurements for several high J lines between J = 55 and 60, we have been able to estimate the following upper bounds for the ν_1 band:

$$\gamma - \gamma^0 < 1 \times 10^{-10} \text{ cm}^{-1},$$

$$\epsilon - \epsilon^0 \leq 2 \times 10^{-11} \text{ cm}^{-1} \qquad (\text{for } J = 55 \text{ and resolution } 0.0034).$$

The only difficulty encountered in fitting the hot-band spectrum was in assigning J for these weak transitions. Fortunately the data provides us with several groups of transitions spaced fairly far apart where the transitions within each group were separated by unit changes in J. Again using trial and error, we found a unique assignment of J for the low-J transitions that correctly predicted the intervals for the observed transitions at higher J. Based on these assignments, a two-parameter fit of 11 measured hot-band transitions resulted in the values

$$\alpha' = 909.1997 \pm 0.0003 \text{ cm}^{-1},$$

$$(\beta - \beta^0)' = (-3.405 \pm 0.004) \times 10^{-4} \text{ cm}^{-1}$$

with a 6.5×10^{-4} cm^{-1} rms deviation for the 11 points. The proximity of this $(\beta - \beta^0)$ term to that for the ν_1 band is remarkable. Table II lists the observed and calculated line positions for this hot-band spectrum, along with line intensities.

TABLE I

Transition Frequencies and Intensities for the ν_1 Band

J	Observed (cm^{-1})	Calculated (cm^{-1})	Error ($.001\ cm^{-1}$)	Calculated Intensity
0	--	909.0720	--	1
1	--	909.0713	--	2
2	909.0705 [a]	909.0699	0.6	5
3	--	909.0678	--	15
4	909.0646 [a]	909.0650	-0.4	23
5	--	909.0616	--	24
6	909.0571 [a]	909.0574	-0.3	53
7	909.0526 [a]	909.0525	0.0	54
8	909.0480 [a]	909.0470	1.0	67
9	909.0419 [a]	909.0407	1.1	94
10	909.0340	909.0338	0.2	110
11	909.0268	909.0262	0.7	110
12	909.0180	909.0178	0.2	160
13	909.0094	909.0088	0.6	160
14	908.9986	908.9991	-0.5	177
15	908.9887	908.9887	-0.0	214
16	908.9778	908.9776	0.2	231
17	908.9655	908.9657	-0.3	227
18	908.9528	908.9533	-0.4	286
19	908.9399	908.9401	-0.2	281
20	908.9256	908.9262	-0.6	296
21	908.9115	908.9116	-0.1	332
22	908.8961	908.8963	-0.2	345
23	908.8804	908.8803	0.1	334
24	908.8634	908.8637	-0.3	390
25	908.8459	908.8463	-0.5	376
26	908.8280	908.8283	-0.2	384
27	908.8094	908.8095	-0.1	412
28	908.7901	908.7801	0.0	416
29	908.7702	908.7699	0.3	398
30	908.7489	908.7491	-0.2	441
31	908.7277	908.7276	0.1	421
32	908.7058	908.7054	0.4	419
33	908.6833	908.6825	0.9	435
34	908.6590	908.6589	0.1	430
35	908.6348	908.6345	0.3	406
36	908.6097	908.6096	0.1	434
37	908.5838	908.5839	-0.1	408
38	908.5571	908.5575	-0.3	399
39	908.5302	908.5304	-0.1	404
40	908.5026	908.5026	-0.0	392
41	908.4745	908.4742	0.4	365
42	908.4451	908.4450	0.1	379
43	908.4154	908.4151	0.2	352
44	908.3845	908.3846	-0.1	338
45	908.3532	908.3533	-0.1	335
46	908.3216	908.3214	0.2	319
47	908.2889	908.2888	0.2	294
48	908.2555	908.2554	0.1	298
49	908.2210	908.2214	-0.4	273
50	908.1866	908.1867	-0.1	258
51	908.1510	908.1513	-0.3	251
52	--	908.1152	--	236
53	--	908.0784	--	215
54	--	908.0409	--	212
55	908.0018	908.0027	-0.9	193
56	907.9641	907.9638	0.3	180
57	907.9240	907.9242	-0.2	171
58	--	907.8840	--	159
59	--	907.8430	--	143
60	--	907.8013	--	139

a. Blended peak not included in spectral fit.

The identification of the hot band depends on the fact that at 300 K there is 25% of the population in the ν_2 band relative to the ground state as compared to 15% in the ν_4 band. The spectral intensity ratios best correspond to the ν_2 hot band. The anharmonic constant X_{12} is then

$$X_{12} = \alpha' - \alpha = 0.1277 \pm 0.0003\ \text{cm}^{-1}.$$

This constant was predicted by Jeannotte *et al.* (*8*) to be 0.92, whereas their value of X_{14} was 0.16.

The discrepancy between our experimental value for X_{12} and the calculated value in Ref. (*8*) is a result of the near resonance of $2\nu_2$ and ν_1. The expression for X_{12} can be written as (*9*):

$$X_{12} = d_{1122} + \frac{2C_{122}^2\omega_2}{\omega_1^2 - (2\omega_2)^2} - \frac{3C_{111}C_{122}}{\omega_1},$$

TABLE II

Transition Frequencies and Intensities for the $\nu_1 + \nu_2 \leftarrow \nu_2$ Hot Band

J	Observed (cm^{-1})	Calculated (cm^{-1})	Error ($.001\ cm^{-1}$)	Calculated Intensity
0	--	909.1997	--	0
1	--	909.1990	--	0
2	--	909.1977	--	1
3	--	909.1956	--	4
4	--	909.1929	--	6
5	--	909.1895	--	6
6	--	909.1854	--	13
7	--	909.1807	--	13
8	--	909.1752	--	17
9	--	909.1691	--	23
10	--	909.1623	--	27
11	--	909.1548	--	27
12	909.1476	909.1466	1.0	40
13	909.1377	909.1377	-0.1	39
14	909.1273	909.1282	-0.9	44
15	909.1169	909.1180	-1.0	53
16	909.1071	909.1071	0.0	57
17	909.0958	909.0955	0.3	56
18	909.0838	909.0833	0.5	71
19	--	909.0703	--	69
20	--	909.0567	--	73
21	--	909.0424	--	82
22	--	909.0274	--	85
23	--	909.0117	--	83
24	--	908.9954	--	96
25	--	908.9784	--	93
26	--	908.9607	--	95
27	--	908.9423	--	102
28	--	908.9232	--	103
29	908.9039	908.9034	0.5	98
30	--	908.8830	--	109
31	--	908.8619	--	104
32	--	908.8401	--	103
33	908.8174	908.8176	-0.2	107
34	--	908.7945	--	106
35	--	908.7706	--	100
36	--	908.7461	--	107
37	--	908.7209	--	101
38	908.6953	908.6950	0.2	99
39	908.6682	908.6685	-0.3	100
40	--	908.6412	--	97
41	--	908.6133	--	90
42	--	908.5847	--	94
43	--	908.5554	--	87
44	--	908.5254	--	83
45	--	908.4948	--	83
46	--	908.4635	--	79
47	--	908.4315	--	73
48	--	908.3988	--	74
49	--	908.3654	--	68
50	--	908.3313	--	64
51	--	908.2966	--	62
52	--	908.2612	--	58
53	--	908.2251	--	53
54	--	908.1883	--	52
55	--	908.1508	--	48
56	--	908.1127	--	44
57	--	908.0739	--	42
58	--	908.0344	--	39
59	--	907.9942	--	35
60	--	907.9533	--	34

where the C and d terms are cubic and quartic potential constants, respectively. The second term above is large, because of the near resonance ($\omega_2 \sim 435\ cm^{-1}$ and $\omega_1 \sim 910\ cm^{-1}$), and must be positive, thus accounting for the sign of X_{12}. However, the magnitude of X_{12} is difficult to calculate because of cancellations with the other terms.

With the line positions calculated, all that is needed to simulate the spectrum is to calculate intensities from the appropriate Boltzmann and spin statistics formulas and add a lineshape function. The Boltzmann factors as a function of J are calculated using the ground-state β value (*10*) of $0.191\ cm^{-1}$. For the hot-band population we have assumed that we are dealing with population in ν_2, which, at $435\ cm^{-1}$, is the lowest frequency mode in the molecule. Relative intensities as a function of J for both the fundamental and the hot band are of course the same, and are the product of $2J + 1$ times the spin statistical weight calculated for a tetrahedral

molecule composed of spin-1/2 nuclei. For high J these weights approach $4(2J + 1)/3$ as a limit.

The Doppler and pressure widths (FWHM) at 300 K and 4 Torr are calculated to be 0.0012 and 0.0013 cm^{-1}, respectively (*11*), which results in a Voight profile considerably narrower than our laser's spectral width. Thus, in order to simulate the spectrum, we have synthesized a Voight profile with a Gaussian component of 3.4×10^{-3} cm^{-1}, which includes 90 MHz for the linewidth of our laser sources. Calculated spectra based on these parameters are shown in Figs. 1b and 2b. The close similarity of the observed and calculated intensities provides additional verification of our assignment of J in both the fundamental and hot-band spectra. The agreement with the observed relative intensities of the two bands also supports our assumption of a ν_2 hot band.

CONCLUSIONS

We have obtained the fundamental spectroscopic constants for both the ν_1 fundamental and the $\nu_1 + \nu_2 \leftarrow \nu_2$ hot band of CF_4 which fit the observed spectrum with an accuracy significantly better than 10^{-3} cm^{-1}. By so doing, we have illustrated the use of inverse Raman spectroscopy as a general, ultra-high-resolution spectroscopic tool that should be of particular importance in the detailed spectroscopic study of even larger, heavier, and more complex molecules. Unfortunately, we have been unable to observe any additional hot-band structure over the 2-cm^{-1} interval beyond the ν_1 band origin, therefore limiting our positive identification of the ν_2 band. Our tentative assignment of the observed hot band is thus based entirely on its intensity relative to the fundamental band.

ACKNOWLEDGMENTS

We would like to thank Drs. B. J. Krohn, A. V. Smith and J. M. Hoffman for helpful discussions. We gratefully acknowledge the expert technical assistance of R. E. Asbill.

RECEIVED: June 2, 1980

REFERENCES

1. A. OWYOUNG, C. W. PATTERSON, AND R. S. MCDOWELL, *Chem. Phys. Lett.* **59**, 156–162 (1978); **61**, 636 (1979).
2. R. S. MCDOWELL, C. W. PATTERSON, AND A. OWYOUNG, *J. Chem. Phys.* **72**, 1071–1076 (1980).
3. A. OWYOUNG, *in* "Laser Spectroscopy IV" (H. Walther and R. W. Rothe, Ed.), pp. 175–187, Springer-Verlag, Berlin, 1979.
4. L. RAHN AND A. OWYOUNG, to be published.
5. J. A. ARMSTRONG, J. J. WYNNE, AND P. ESHERICK, *J. Opt. Soc. Amer.* **69**, 211–230 (1979).
6. F. V. KOWALSKI, R. T. HAWKINS, AND A. L. SCHAWLOW, *J. Opt. Soc.* **66**, 965–966 (1976); B. W. PETLEY AND K. MORRIS, *Opt. Quant. Electron.* **10**, 277–278 (1978).
7. J. MORET-BAILLY, *Cah. Phys.* **15**, 237–314 (1961); *J. Mol. Spectrosc.* **15**, 344–354 (1965).
8. A. C. JEANNOTTE II, C. MARCOTT, AND J. OVEREND, *J. Chem. Phys.* **68**, 2076–2084 (1978).
9. K. T. HECHT, *J. Mol. Spectrosc.* **5**, 335–389 (1960).
10. C. W. PATTERSON, R. S. MCDOWELL, N. G. NERESON, R. F. BEGELY, H. W. GALBRAITH, AND B. J. KROHN, *J. Mol. Spectrosc.* **80**, 71–85 (1980).
11. C. W. PATTERSON AND R. S. MCDOWELL, *Proc. Soc. Photo.-Opt. Instrum. Eng.*, in press.